

Towards a NMR Implementation of a Quantum Lattice Gas Algorithm

Marco A. Pravia¹, Zhiying Chen¹, Jeffrey Yezep², David G. Cory^{1*}

¹ Department of Nuclear Engineering, Massachusetts Institute of Technology, Cambridge, MA 02139

² Air Force Research Laboratory, Hanscom Field, MA 01731

August 20, 2001

Abstract

Recent theoretical results suggest that an array of quantum information processors communicating via classical channels can be used to solve fluid dynamics problems. Quantum lattice-gas algorithms (QLGA) running on such architectures have been shown to solve the diffusion equation, the Schrödinger equation, and the Dirac equation. In this report, we describe progress towards an ensemble nuclear magnetic resonance (NMR) implementation of a QLGA that solves the diffusion equation. The methods rely on NMR techniques to encode an initial mass density into an ensemble of two-qubit quantum information processors. Using standard pulse techniques, the mass density can then be manipulated and evolved through the steps of the algorithm. We provide the experimental results of our first attempt to realize the NMR implementation. The results qualitatively follow the ideal simulation, but the observed implementation errors highlight the need for improved control.

1 Introduction

The field of quantum information processing (QIP) has made steady progress over the past decade, driven in part by the realization that some quantum algorithms offer a computational advantage over the best known classical counterparts[1]. To reach a practical improvement, however, most quantum algorithms require a large number of qubits coupled quantum mechanically, thus making physical implementation difficult. Recently, however, it has been suggested that some interesting problems might be solvable by a hybrid classical-quantum device defined as a type-II quantum computer[2]. A type-II quantum computer is essentially a parallel lattice of small quantum information processors that share information through classical channels. Such a device offers the experimental

simplification that quantum coherences need only be maintained locally within each small quantum processor. Using this architecture, it might be possible to increase the range of problems that small quantum processors can tackle by classically stringing many of them together. A type-II quantum computer may thus serve as an intermediate architecture between few-qubit and large-scale quantum computers.

In this report, we explore the experimental aspects of building a type-II quantum computer using nuclear magnetic resonance (NMR) techniques. Quantum information processing by NMR usually employs a liquid sample of molecules containing spin- $\frac{1}{2}$ nuclei and that is subjected to a strong magnetic field[3]. A typical field B_0 of ~ 10 T creates an energy difference ΔE between the aligned and antialigned spin states sufficient to drive the system to an equilibrium state with net magnetization. At room temperature, $\Delta E/kT$ is about 10^{-6} , so that the net magnetization is relatively small, but, given the large number of molecules in the sample ($\sim 10^{18}$), it is still easily detectable. The entire spin ensemble is accurately described by a reduced density matrix of only the intramolecular spin degrees of freedom. The ensemble nature of the NMR sample thus makes it inherently applicable to parallel computation. A type-II architecture can be mapped onto a NMR sample by creating a correspondence between the sites of the lattice and spatially distinct spin ensembles. Using magnetic field gradients and radiofrequency (RF) pulses, information in the lattice can be encoded, manipulated, and read out. As a first test of the NMR implementation, we chose a basic quantum lattice gas algorithm (QLGA) that solves diffusive dynamics in one dimension.

*To whom correspondence should be addressed. E-mail: dcory@mit.edu

2 Lattice-Gas System

The diffusion of a mass density ρ is governed by

$$\frac{\partial \rho}{\partial t} = D \frac{\partial^2 \rho}{\partial t^2} \quad (1)$$

The above equation corresponds to the macroscopic effective field theory result. Its relation to the lattice-gas dynamics is seen by breaking space into an array of lattice sites with occupation probabilities assigned to each site[4, 5]. The ensemble average mesoscopic dynamics are controlled by the transport equations

$$f_1(n, m+1) = f_1(n, m) + \frac{1}{2}[f_2(n, m) - f_1(n, m)] \quad (2)$$

$$f_2(n, m+1) = f_2(n, m) - \frac{1}{2}[f_2(n, m) - f_1(n, m)] \quad (3)$$

where f_1 and f_2 represent occupation probabilities and the bracketed terms represent a collision operator. The mass density ρ is the sum of f_1 and f_2 . The indices n and m correspond to lattice site and time step, respectively. The connection between the diffusion equation and the transport equations may be seen by taking the Chapman-Enskog expansion of the lattice Boltzmann equation written in terms of occupation probabilities.

3 Quantum Lattice-Gas Algorithm

The quantum lattice-gas implementation relies on mapping each initial occupation probabilities f_1 and f_2 into the corresponding single-particle states of two quantum bits,

$$|q_{1,2}(n, m)\rangle = \sqrt{f_{1,2}(n, m)}|1\rangle + \sqrt{1 - f_{1,2}(n, m)}|0\rangle \quad (4)$$

where $|q_{1,2}(n, m)\rangle$ are the single-particle states of the first and second qubits, and $|0\rangle$ and $|1\rangle$ correspond to the eigenstates of a two-level system. The resulting two-qubit wave function for a site becomes

$$|\psi(n, m)\rangle = \sqrt{f_1 f_2}|11\rangle + \sqrt{f_1(1-f_2)}|10\rangle + \sqrt{(1-f_1)f_2}|01\rangle + \sqrt{(1-f_1)(1-f_2)}|00\rangle \quad (5)$$

where $|\psi(n, m)\rangle$ spans the Hilbert space of two coupled quantum systems. After initialization, the algorithm calls for a collision operation

$$|\psi'(n, m)\rangle = \hat{U}|\psi(n, m)\rangle \quad (6)$$

carried out via unitary evolution by a ‘‘square-root of swap’’ gate \hat{U} . The gate \hat{U} can be written as

$$\hat{U} = \begin{pmatrix} 1 & 0 & 0 & 0 \\ 0 & \frac{1}{2} - \frac{i}{2} & \frac{1}{2} + \frac{i}{2} & 0 \\ 0 & \frac{1}{2} + \frac{i}{2} & \frac{1}{2} - \frac{i}{2} & 0 \\ 0 & 0 & 0 & 1 \end{pmatrix} \quad (7)$$

in the standard basis. The next step in the computation requires a measurement of the occupation numbers

$$f'_{1,2}(n, m) = \langle \psi'(n, m) | \hat{n}_{1,2} | \psi'(n, m) \rangle \quad (8)$$

where the number operators $\hat{n}_{1,2}$ are defined as

$$\hat{n}_1 = \begin{pmatrix} 1 & 0 & 0 & 0 \\ 0 & 0 & 0 & 0 \\ 0 & 0 & 1 & 0 \\ 0 & 0 & 0 & 0 \end{pmatrix}, \hat{n}_2 = \begin{pmatrix} 1 & 0 & 0 & 0 \\ 0 & 1 & 0 & 0 \\ 0 & 0 & 0 & 0 \\ 0 & 0 & 0 & 0 \end{pmatrix}. \quad (9)$$

The measured occupation numbers f'_1 and f'_2 are then streamed to nearest lattice sites in opposite directions, as given by

$$f_1(n, m+1) = f'_1(n+1, m) \quad (10)$$

$$f_2(n, m+1) = f'_2(n-1, m) \quad (11)$$

The entire diffusion algorithm can be summarized as repeated applications of the following four steps:

1. Initialization of occupation probabilities in each spatially distinct site
2. Application collision operator, \hat{U} , at all sites
3. Readout of the expectation value of the number operators
4. Determination of the new occupation probabilities by streaming to nearest neighbors

4 NMR Implementation

4.1 Mapping to Spin Ensembles

The first step in creating an experiment to study the implementation of type-II quantum computer is to define a mapping of the theoretically required quantum states to a real physical system. In the liquid-state NMR case, the required quantum states $|\psi(n, m)\rangle$ are physically encoded onto spin ensembles described by density matrices $\sigma(n, m)$

$$|\psi(n, m)\rangle \leftrightarrow \sigma(n, m) \quad (12)$$

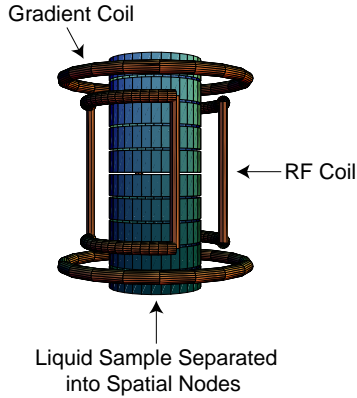


Figure 1: The cylindrical sample of chloroform employed in this experiment is addressed in slices by the combined action of magnetic field gradients and shaped RF pulses. Each slice represents a node in the lattice of quantum information processors

However, the thermal equilibrium of liquid-state NMR systems is a highly mixed state that is not immediately applicable to quantum computing experiments. As a result, the thermal equilibrium state must first be reset to a pseudopure state of the form [6, 7]

$$\sigma(n, m) = 1 - \varepsilon |\psi(n, m)\rangle\langle\psi(n, m)| \quad (13)$$

The above pseudopure state transforms identically to the corresponding pure state $|\psi(n, m)\rangle$. Each subensemble $\sigma(n, m)$ is in turn composed of a large number ($\sim 10^{18}$) of individual molecules distributed within a slice of a cylindrical sample. More formally, the reduced density matrix $\sigma(n, m)$ at a site is

$$\sigma(n, m) = Tr_{\vec{r}} \left[\sum_{\vec{r}} T \left[\frac{z}{\Delta z} - \left(n - \frac{1}{2} \right) \right] |\phi(\vec{r}, m)\rangle\langle\phi(\vec{r}, m)| \right] \quad (14)$$

where $|\phi(\vec{r}, m)\rangle$ is the nuclear spin state of a single molecule located at position \vec{r} , $T(z)$ is the “top hat” function

$$T(z) = \begin{cases} 1, & |z| \leq \frac{1}{2} \\ 0, & |z| > \frac{1}{2} \end{cases} \quad (15)$$

that selects the relevant spatial slice with thickness Δz , and $Tr_{\vec{r}}$ denotes the partial trace over the spatial degree of freedom. The variable z represents the corresponding coordinate of the vector \vec{r} . Figure 1 depicts the geometrical arrangement of the slices relative to the gradient and RF coils in the NMR probe. As evident from the figure and equation 14, a stack of pseudopure states becomes the physical realization of the required lattice.

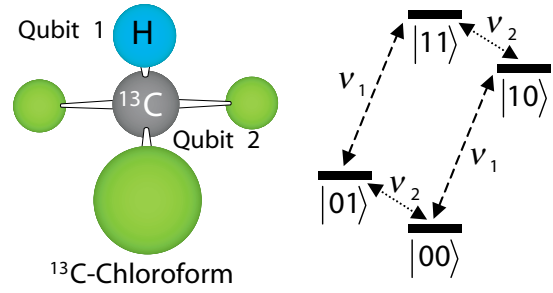


Figure 2: The picture shows the chloroform molecule and the nuclear spin energy level diagram.

4.2 Control and Measurement of Spin System

In our particular test, we implemented a two-qubit diffusion algorithm using a solution of chloroform ($^{13}\text{CHCl}_3$) where the hydrogen and the labeled carbon nuclei served as qubits 1 and 2, respectively. Figure 2 shows the energy level diagram of the spins and a picture of the molecule. As shown in the diagram, the proton splitting is four times larger than the carbon splitting, and both splittings are a small fraction of kT .

In the absence of a magnetic field gradient, the Hamiltonian of the spin system in the doubly-rotating frame is

$$H(t) = \frac{\pi J}{2} \sigma_z^1 \sigma_z^2 + [w_x^1(t) \sigma_x^1 + w_y^1(t) \sigma_y^1] + [w_x^2(t) \sigma_x^2 + w_y^2(t) \sigma_y^2] \quad (16)$$

The first term denotes the scalar interaction between the spins, while the remaining terms are the externally-controlled RF Hamiltonian. The operators of the form $\sigma_{x,y,z}^{1,2}$ are Pauli spin matrices corresponding to each qubit, and the scalar coupling Hamiltonian is a Kronecker product of the single-spin operators. The RF part of the Hamiltonian generates arbitrary single spin rotations with high fidelity when the nutation rates $w_{x,y}^{1,2}$ are much stronger than J , the scalar coupling constant.

As mentioned before, the collision operator \hat{U} for this algorithm is the square-root of swap gate. The unitary operator \hat{U} can be written as

$$\hat{U} = \exp \left[-i \frac{\pi}{8} (\sigma_x^1 \sigma_x^2 + \sigma_y^1 \sigma_y^2 + \sigma_z^1 \sigma_z^2) \right] \quad (17)$$

if an irrelevant phase is ignored. Written in this form, it is clear that \hat{U} can be decomposed into the product

Diffusion Equation

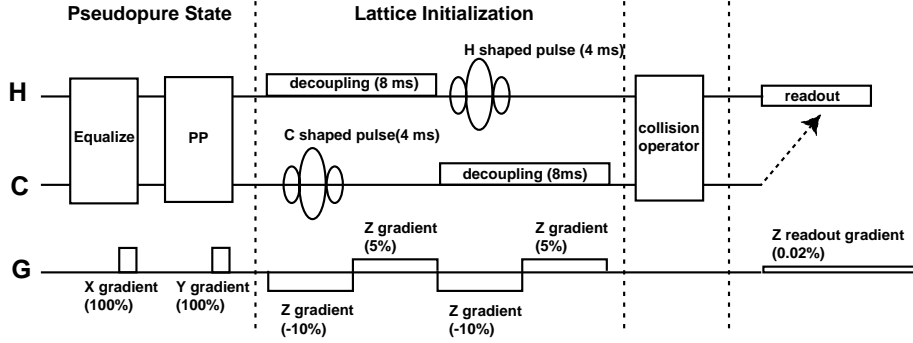


Figure 3: The pulse sequence for a single time step of the algorithm begins with the pseudopure state preparation. Gradients are used to perform the necessary nonunitary operations required for equalizing the magnetization of the two spin species and to prepare the pseudo pure state. The lattice initialization is accomplished by applying weak RF shapes in the presence of a magnetic field gradient in the Z direction. A decoupling sequence prevents the scalar coupling from interfering with the initialization. The collision operation is performed by a sequence of coupling delays and strong RF pulses. The collision pulse sequence is applied without a gradient so that all of the spins in the lattice feel the same operation. Readouts of both the carbon and hydrogen magnetizations are carried out on the hydrogen channel in two separate experiments.

of three commuting terms. Each term can be implemented by making use of the scalar coupling Hamiltonian plus appropriate single-spin rotations[8]. The operator \hat{U} is applied to all the subensembles $\sigma(n, m)$ such that

$$\sigma'(n, m) = \hat{U}\sigma(n, m)\hat{U}^\dagger \quad (18)$$

in analogy with equation 6.

The final steps of the algorithm are to read the occupation numbers encoded in $\sigma'(n, m)$ and to stream them to nearby sites. The readout is accomplished by noticing that equation 8 can be rewritten in terms of the z -Pauli matrices as

$$\begin{aligned} f'_{1,2}(n, m) &= \langle \psi'(n, m) | \frac{1 - \sigma_z^{1,2}}{2} | \psi'(n, m) \rangle \quad (19) \\ &= \frac{1}{2} \left[1 - \langle \psi'(n, m) | \sigma_z^{1,2} | \psi'(n, m) \rangle \right] \end{aligned}$$

using the fact that $\hat{n}_{1,2} = \frac{1}{2}(1 - \sigma_z^{1,2})$. The last equation can be written in the final form

$$f'_{1,2}(n, m) = \frac{1}{2} \left[1 - M_z^{1,2} \right] \quad (20)$$

where the trace has been replaced by the z -magnetization $M_z^{1,2}$. The z -magnetization is easily measured in NMR by applying a “read” $\pi/2$ pulse and observing the transverse magnetization. The measured values $f'_{1,2}$ can be streamed on a classical computer and then reinitialized onto the lattice.

4.3 Pulse Sequence

The diagram in figure 3 shows the main parts of a single time step of the NMR implementation: pseudopure state preparation, lattice initialization, collision, and readout. The top two lines correspond to operations on the two qubits (H and C), while the third line shows the required gradient pulses. The pseudopure state was prepared by first equalizing the magnetizations of the two spins, followed by a pseudopure state creation sequence[9]. The starting occupation numbers for each time step were then encoded using weak shaped RF pulses on the two spins applied simultaneously with a linear magnetic field gradient. Because the total RF nutation angle was small, the shape of the pulse was determined by taking the Fourier transform of the desired magnetization profile[10]. This step is related to slice-selection in magnetic resonance imaging(MRI). A decoupling sequence was applied simultaneously with the RF shape, thus averaging out the effects of the scalar coupling on the RF excitation.

The collision operator was implemented by decomposing \hat{U} into sequences of scalar coupling delays and RF pulses. The final readout was performed by recording the spectra in the presence of a weak gradient. The classical communication part of the algorithm was absorbed into the encoding operation for the subsequent time step. A linear phase ramp was added to the RF shape, effectively shifting the frequency of the excitation. Since the data on the two spins was to be shifted in different directions, the phase ramps for the two RF

pulses had opposing slopes.

5 Results

The two figures 4 and 5 below show the results of preliminary experiments and, for comparison, the corresponding ideal simulation of the NMR implementation. The experiments were performed using 16 nodes iterated through 12 time steps of the algorithm. As can be seen, the broad features of the diffusion can be seen, but large errors are present in the implementation. The errors are caused by problems in the decoupling sequence, errors in the Fourier transform approximation, and other experimental imperfections. We are continuing to refine the experiments and we expect to correct these errors in the near future with improved results to be published in a subsequent paper [11].

6 Conclusion

Ensemble NMR techniques have been successfully used to study the experimental details involved in quantum information processing. The astronomical number of individual quantum systems ($\sim 10^{18}$) present in typical liquid-state spin ensembles greatly facilitates the problem of measuring spin quantum coherences. In addition, the ensemble nature has been successfully utilized to create the necessary pseudopure states and to systematically generate nonunitary operations over the ensemble[12]. In this implementation, we again exploit the ensemble nature, but this time as a means of realizing a lattice of quantum information processors. The implementation combines the advantages of quantum computation at each node with parallel computation throughout the lattice. The large size of the NMR ensemble provides, in principle, sufficient room to explore large lattices. Although achieved experimental results point to the need for better control, the experiments are a first step towards realizing the quantum lattice gas algorithm on a NMR quantum information processor.

7 Acknowledgements

References

[1] C.H. Bennett, D.P. DiVincenzo, *Nature* **404** 247-55 (2000)

- [2] J. Yepez, *International Journal of Modern Physics C* **12** (9) 1273-84 (2001)
- [3] R.R. Ernst, G. Bodenhausen, and A. Wokaun, *Principles of Nuclear Magnetic Resonance in One and Two Dimensions*, Oxford University Press, Oxford (1994)
- [4] J. Yepez, *International Journal of Modern Physics C* **12** (9) 1285-303 (2001)
- [5] J. Yepez, *International Journal of Modern Physics C* **9** (8) 1587-96 (1998)
- [6] D.G. Cory, A.F. Fahmy, T.F. Havel, *Proceedings of the National Academy of Sciences* **94** (5) 1634-39 (1997)
- [7] N.A. Gershenfeld, I.L. Chuang, *Science* **275** 350-56 (1997)
- [8] D.G. Cory, M.D. Price, T.F. Havel, *Physica D* **120** (1-2) 82-101 (1998)
- [9] M. Pravia, E. Fortunato, Y. Weinstein, M.D. Price, G. Teklemariam, R.J. Nelson, Y. Sharf, S. Somaroo, C.H. Tseng, T.F. Havel, D.G. Cory, *Concepts in Magnetic Resonance* **11** (4) 225-38 (1999)
- [10] A. Sodickson and D.G. Cory, *Progress in Magnetic Resonance* **33** 78-108 (1998)
- [11] M.A. Pravia, Z. Chen, J. Yepez, D.G. Cory, manuscript in preparation for 2002.
- [12] T.F. Havel, Y. Sharf, L. Viola, D.G. Cory, *Physics Letters A* **280** (5-6) 282-8 (2001)

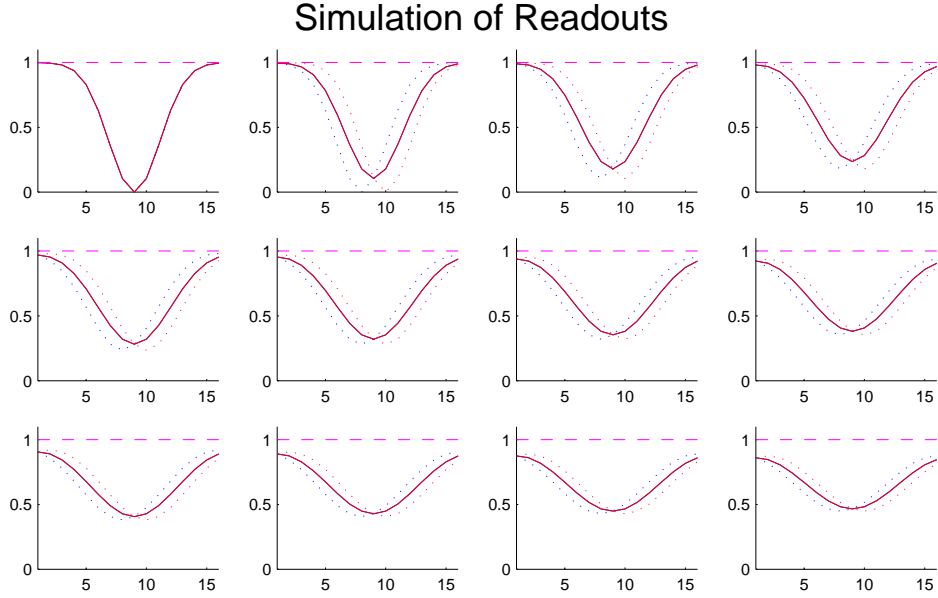


Figure 4: The plots show a simulated run of the ideal quantum lattice gas algorithm for diffusion. The top left plot contains the first step, followed to the right and then down the rows by subsequent time steps. The dotted lines represent the initialized occupation numbers $f_{1,2}$ for each spin, while the solid lines represent the occupation numbers $f'_{1,2}$ present after the collision. The x-axis labels the node number and runs from 1 to 16.

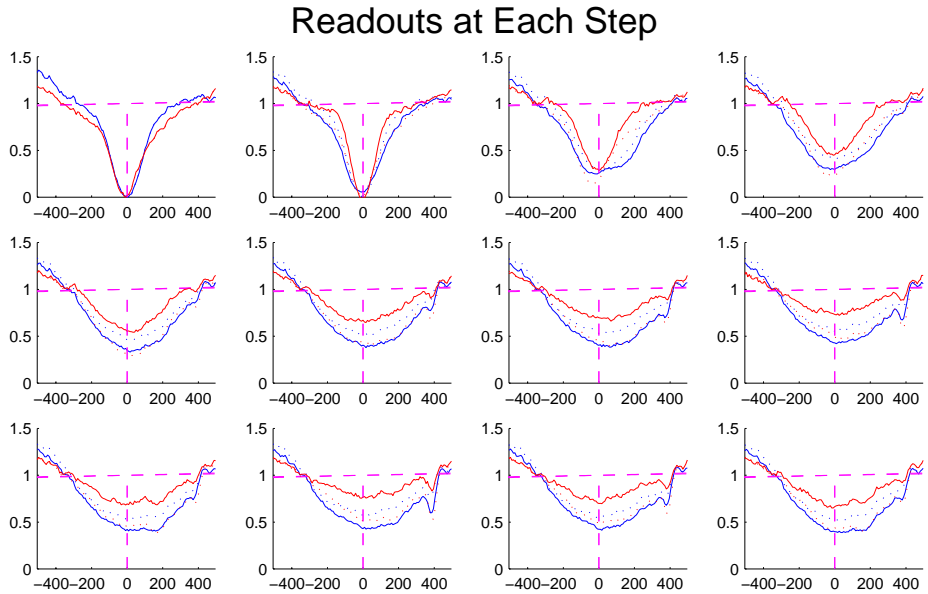


Figure 5: The experimental results for the corresponding time steps of the simulations from figure 4. Although the general features follow the simulation, the experimental results are not of high fidelity and suggest a need for more precise control. The x-axis labels the observed spectral frequency. The actual nodes used in the experiment reside in the region between -200 Hz and 200 Hz. The outlying region is included for reference.